RECENT EXTENSIONS TO THE FREE-VORTEX-SHEET THEORY FOR EXPANDED CONVERGENCE CAPABILITY

James M. Luckring
NASA Langley Research Center
Hampton, Virginia

Keith D. Hoffler
Vigyan Research Associates, Inc.
Hampton, Virginia

Arthur C. Grantz
Northrop Corporation
Hawthorne, California

SUMMARY

A new version of the free-vortex-sheet formulation is presented which has greatly improved convergence characteristics for a broad range of geometries. The enhanced convergence properties were achieved largely with extended modeling capabilities of the leading-edge vortex and the near-field trailing wake. Results from the new code, designated FVS-1, are presented for a variety of configurations and flow conditions with emphasis on vortex flap applications.

INTRODUCTION

The design constraints for high-speed aircraft with efficient supersonic performance capability often result in highly swept wings which are conducive to separation-induced leading-edge vortex flows at moderate-to-high angles of attack. Although this type of separation can cause increased drag through the loss of leading-edge thrust, the vortex-lift characteristics resulting from this highly stable flow can be used to improve takeoff and landing capabilities, provide maneuver lift increments at subsonic and transonic speeds, and, most recently, reduce drag at moderate to high lift coefficients through the use of simple "vortex flaps." As for attached flow, however, the full exploitation of this vortex flow will require improved theoretical analysis and design techniques capable of providing reasonable estimates of the three-dimensional surface pressure distributions at a practical expenditure of human and computer resources.

However, the computation of these vortex flow effects has proven to be a challenging task. It is only during the last 10 years or so that methods have begun to emerge with the stated capability, even for simple three-dimensional geometries with sharp leading edges at subsonic speeds. Among these methods, the free-vortex-sheet theory has provided the best estimates of the inviscid surface pressure distributions for a rather broad class of generic wing shapes. The major drawback of this method has proven to be the difficulty often encountered in achieving converged results.

A new version of the free-vortex-sheet formulation, designated FVS-1, is presented in this paper which has greatly improved convergence properties for a broad range of geometries including vortex flaps. The convergence difficulties were approached from a fluid-mechanical viewpoint as opposed to that of numerical analysis. As a consequence, the basic numerical method for iteratively solving the nonlinear vortex flow problem required little change. The enhanced convergence properties were achieved largely with extended modeling capabilities of the leading-edge vortex and the near-field trailing wakes. Using this approach, considerable insight was gained into the underlying fluid mechanics of vortex modeling as related to convergence considerations. Results are presented which demonstrate the expanded convergence capabilities with emphasis on the salient features modeled as well as the aerodynamic consequences of these modeling techniques.

SYMBOLS

AR	aspect ratio
b	wing span
C_B	static root bending moment coefficient, static root bending moment/$(q_\infty S_{ref} b)$
C_D	drag coefficient, drag/$(q_\infty S_{ref})$
$C_{D,o}$	experimental value of drag coefficient at $C_L = 0$
ΔC_D	drag-due-to-lift coefficient, $C_D - C_{D,o}$
C_L	lift coefficient, lift/$(q_\infty S_{ref})$
C_m	pitching moment coefficient, pitching moment/$(q_\infty S_{ref} \bar{c})$
C_N	normal force coefficient, normal force/$(q_\infty S_{ref})$
C_p	static pressure coefficient, $(p - p_\infty)/q_\infty$
ΔC_p	$C_{p,u} - C_{p,l}$
c	streamwise chord
$\bar{c}$	reference chord
c_r	root chord
c_t	tip chord
E	log (Σr^2)
It	iteration number
ℓ_{nw}	longitudinal extent of near wake in fraction of vortex-core diameter at trailing edge

M	Mach number
N_{up}	number of update iterations
$\hat{n}$	unit normal vector
p	static pressure; also maximum camber height in fraction local semispan
q_∞	freestream reference dynamic pressure, $(1/2)\ \rho_\infty\ U_\infty^2$
r	individual panel residual error
S_{ref}	reference area
s	local semispan
t	thickness
U_∞	freestream reference velocity
(u,v,w)	perturbation velocity components
(x,y,z)	body-axis Cartesian coordinates
α	angle of attack, degrees
α_{so}	angle of attack for smooth onflow
$\Delta\alpha$	$\alpha - \alpha_{so}$
β	angle of sideslip, degrees; also, Prandtl-Glauert factor, $(1 - M_\infty^2)^{1/2}$
δ	deflection angle, degrees, positive downward
δ_f	vortex flap deflection angle normal to hingeline, degrees, positive downward
$\Delta\delta_f$	increment in δ_f
δ_t	side-edge rake angle, degrees, positive inboard
Λ	sweep angle, degrees
λ	taper ratio, c_t/c_r
ρ_∞	freestream reference density
Σ	summation
$\vec{\zeta}$	vorticity vector
$\cdot$	vector dot product
$\|\|$	vector magnitude

Subscripts

f	flap
hl	hingeline
l	lower surface
le	leading edge
te	trailing edge
u	upper surface
1	first order in perturbation quantities; also, inboard
2	second order in perturbation quantities; also, outboard
∞	freestream reference conditions

Abbreviations

Arg	argument
FVS	free vortex sheet

CONVERGED FVS PARAMETER SPACE

A study was initially conducted to document the converged parameter space of the free-vortex-sheet method as demonstrated in the open literature. The results are detailed in Table 1 and partially summarized in figure 1. In Table 1, the results are organized by planform type, first for flat wings and then for cambered wings; within one class of planform and camber they are listed alphabetically by first author. It should be noted that most entries correspond to a range of solutions obtained for a systematic variation of some salient parameter such as angle of attack, Mach number, sweep angle, flap deflection angle, etc. Although a number of significant aspects of this solution space could be called out (not to mention details of the solutions themselves), the main point to be observed is the extent of geometric variation and freestream conditions over which the method has been successfully applied.

Some general features of free-vortex-sheet solutions are highlighted in figure 2. By virtue of explicitly modeling the leading-edge vortex, a variety of "real flow" effects are included in the FVS solutions which, to date, have not been calculable by simpler methods. The chief feature of these solutions is an accurate estimation of the three-dimensional, inviscid pressure field. By way of integration this also results in accurate force and moment estimates. In addition, high angle-of-attack vortex lift loss effects due to longitudinal vortex curvature near the trailing edge as well as vortex crowding are implicitly represented. Additional discussion of these effects has been given by Polhamus (1983, 1985).

Although not covered in this paper, the FVS method has recently been extended to account for two primary effects of viscosity and distributed vorticity, vortex breakdown and secondary vortex separation. (The method is still limited to flows

C-2

with a known primary separation line such as occurs with a sharp leading edge.) By imbedding a parabolized Navier-Stokes representation of an axisymmetric vortex core, Luckring (1985) showed that the condition of incipient vortex breakdown at the trailing edge of delta, arrow, and diamond wings could be predicted with a critical helix angle concept. Wai et al. (1985) demonstrated the first estimations of secondary vortex separation with the FVS method by modeling the upper surface boundary layer flow and interacting the viscous flow effects with the outer inviscid flow. Although continuing development of the vortex core and secondary vortex effects will be required, the initial findings of these studies are quite promising. The current status of secondary separation modeling by boundary layer techniques will be addressed in this conference by Blom et al. (1985) as well as by Woodson and DeJarnette (1985).

METHOD EXTENSIONS

From the experience gained in utilizing the free-vortex-sheet method, four aspects of the formulation were chosen for modification. The first three aspects regard flow modeling considerations; they are the near-wake model, the restart capability, and the manipulation of the starting vortex sheet geometry. The fourth aspect regards the quasi-Newton scheme employed to solve the nonlinear system of governing equations.

Near-Wake Considerations

The primary attributes of the near-wake flow field are summarized in figure 3 for the conditions of planar and nonplanar vorticity. In either case, the trailing-edge Kutta condition results in a near-wake flow which is tangent to the wing at the trailing edge. For planar vorticity the linear form of the pressure coefficient is appropriate and, when taken in conjunction with the no-load wake boundary condition, results in a wake flow where the magnitude of the vorticity vector is free, but its argument is fixed at the streamwise direction.

As is true for slender-body theory, nonplanar vorticity necessitates the inclusion of nonlinear terms in the equation for the pressure coefficient. Although these terms are second order in form, their contribution is of first order, particularly with regard to the sidewash (v). Employing this more exact form of the pressure coefficient in conjunction with the no-load wake boundary condition yields a more realistic wake flow where both the magnitude and the argument of the vorticity vector are now free quantities. These effects allow the wake vorticity to skew laterally and significantly affect the satisfaction of the trailing-edge Kutta condition as was shown by Luckring et al. (1982), for leading-edge vortex flows. However, it must be emphasized that the driving mechanism of this wake effect is the presence of nonplanar vorticity, only one example of which is the leading-edge vortex problem. Other examples of conditions where these effects would also be important include wings with significantly nonplanar geometries such as wings with winglets or vortex flaps, regardless of whether the flow is attached or separated.

An example of the nonplanar effect is presented in figure 4 in the form of vorticity contours. Although both calculations utilized the higher order near wake, the attached flow case of figure 4a resulted in the wake vorticity orienting itself largely in the streamwise direction since the vorticity of this flow is planar. Here, it is evident that the conventional approximations made for the simple trailing wake are adequate for this flow. In the nonplanar vortex-flow case of

figure 4b the lateral skewing of the wake vorticity is significant; modeling this flow with a simple trailing wake would constitute a poor approximation. It is of interest to note the coalescence of vorticity downstream in the near wake. This is indicative of the wake vortex which occurs on slender wings with leading-edge separation; it is shed along the trailing edge and has the opposite sense of the leading-edge vortex.

From a convergence viewpoint, it is desirable to make the near wake as short as possible while maintaining the beneficial effects of this model. A long near wake would not only require more panels (increasing computational expense) but also require increasingly complicated wake flow effects to be represented, hampering convergence. Fortunately, the results of a near-wake length study (figure 5) show very little effect of the length of near wake modeled on the converged force and moment properties of a delta wing. In this figure, the near-wake length is presented in fractions of the vortex core diameter at the wing trailing edge. Also shown are the suction analogy estimates of the normal force coefficient for two angles of attack. Apparently the salient feature of the higher order near wake is to allow the wing vorticity to pass onto the wake with the proper orientation. As has been shown in other studies, details of the wake rollup have little effect on the wing flow itself. Additional calculations (not shown) indicated little sensitivity of the solution to near-wake paneling variations at a fixed near-wake length.

A comparison of the convergence histories for a wing with no near wake and a wing with a short near wake is shown in figure 6. Both solutions required eight iterations to drive the residual error below a tolerence of 10^{-6}, and the overall character of the convergence was unchanged by adding the short near wake. It is noteworthy that the consequences of modeling nonplanar vorticity effects with the near wake have a larger effect on the solution than does driving the residual error down 10 orders of magnitude from unacceptable to fully acceptable levels.

The results of figure 6 also indicate that the overall force and moment coefficients are converged at a residual error level on the order of 10^{-3}, as opposed to the default tolerance of 10^{-6}. In figure 7, the effect of the residual error level on the spanwise pressure distributions very near the trailing edge (where convergence is generally slowest) also indicate that 10^{-3} is acceptable for practical applications. Examination of the other calculations of this paper further supports this conclusion.

Computed force and moment properties for the unit-aspect-ratio delta wing of Hummel (1979) are compared with experimental values in figure 8. The wing was represented by mean plane doublet networks to account for the asymmetric beveling and thickness effects were not modeled. The calculations (with a short near wake) show excellent agreement with the experiment including camber effects which, for the most part, are due to the trailing-edge bevel (a trailing-edge-flap type of effect). Solutions were obtained down to relatively low angles of attack (in magnitude) and lift coefficients; at ±5 degrees the computed vortex-lift increment was approximately ±0.03 from the computed attached flow value. (The attached flow solutions are for zero leading-edge suction.)

Spanwise pressure distributions for 20° angle of attack correlate reasonably well with the experimental results (figure 9). Differences on the upper surface in peak suction magnitude and in the outboard values are largely due to secondary separation, a viscous flow effect. At the aft station shown, thickness effects also affect the quality of the correlation. This is the station of maximum thickness,

and the thin wing calculations reflect the singular nature of the modeled flow at this station.

Partial Restart

A quasi-Newton method is used to solve the nonlinear equations for the free-vortex-sheet formulation. As with any Newton method, the starting solution must be "sufficiently close" to the converged answer if that answer is to be achieved. The basic FVS code has a full restart capability which is useful for changes in the far-field boundary conditions. Here the complete solution (singularities and vortex geometry) from a prior calculation is used as a starting solution for a new calculation of the same wing geometry (and paneling) at different freestream conditions. This capability has proven to be very useful and cost effective for computations over a range of freestream conditions such as angle of attack, Mach number, etc., and was used for the results of the Hummel delta wing just discussed. For cases where no prior information is available, the default approach was to base the initial vortex-sheet geometry on the conical-flow solution of Smith (1966) and to calculate the initial singularity distribution from a subset of the full governing equations.

The restart capability of this method has been extended to include a "partial restart" which is useful for changes in the near-field boundary conditions such as would arise for a change in wing geometry, paneling, etc. The partial restart allows for the transfer of an arbitrary vortex sheet geometry from some prior calculation to the current configuration of interest and solves for the initial singularity distribution by satisfying a subset of the full governing equations. This technique has been exploited for many of the vortex-flap solutions summarized in Table 1, primarily for achieving solutions over a range of vortex-flap deflection angles. However, it was found that the utility of the partial restart diminished as the differences in boundary conditions between an available and the desired solution increased. For this reason, additional vortex-sheet manipulation capability was implemented.

Vortex Sheet Manipulation

For many practical applications the geometric properties of the leading-edge vortex can be dominated by some salient geometric characteristic of the wing. One example is the vortex flap application where the resultant vortex geometries are similar in a coordinate system normal to the flap surface. Therefore, a simple vortex manipulation capability was implemented which allows the initial vortex geometry to be arbitrarily rotated and/or scaled about the wing leading edge. This idea is illustrated in figure 10, where the vortex sheet from an available three-dimensional solution for a planar delta wing is first transferred (via the partial restart) to a wing with a deflected vortex flap, and is then rotated by the flap deflection angle. In practice, it is often advantageous to also slightly scale the resultant initial vortex geometry as well. The effects of this approach on convergence are shown in figure 11a. Use of the simple transfer, rotation, and scaling readily yielded a converged solution for a large increment in flap deflection; for small increments in flap deflection either the transfer alone or in conjunction with manipulation readily yielded the converged solution. Without these techniques converged results had not been achieved.

An example of the scaling effects is illustrated in figure 11b. The converged solution for a delta wing was transferred to the gothic wing and then scaled to

approximate the nonconical effects due to the gothic wing planform. Once again the calculation readily converged; using conical flow information for the starting solution, the prior version of the code would not yield a converged result.

The partial restart and vortex manipulation can be used to obtain solutions for more complex geometries and flow conditions. Shown in figure 12 is an example for a wing-body configuration with a gothic planform vortex flap deflected at a large angle. By organizing the calculations roughly as shown one can obtain intermediate solutions which are useful for interpreting the complete configuration solution as well as for determining incremental effects of geometric variations. In figure 13 an example is shown for a similar wing geometry but at sideslip conditions. Drawing upon simple-sweep concepts, symmetric calculations were first performed which, by the partial restart, provided good starting solutions for the complete configuration.

The approach taken for this case can also be cost effective since the gross solution features are established with the two symmetric calculations which nominally require one-half the computer resources of a full-span calculation for the same paneling and number of iterations. The symmetric precursor calculations could have been performed at reduced panelings, further affecting cost reduction. This feature has been exploited for various problems by initiating a solution with a coarse paneling and then, using the partial restart, obtaining solutions for finer panelings, much as is done with mesh sequencing in finite-difference formulations.

Modified Quasi-Newton Scheme

With the default quasi-Newton scheme of the free-vortex-sheet method the Jacobian matrix is fully formulated at the starting solution and then only every third iteration thereafter. For the intermediate iterations the values of the Jacobian are obtained with an approximate update procedure due to Broyden (1973). By this approach, there is no need to fully reevaluate the partial derivatives comprising the elements of the Jacobian for each iteration. So long as the method converges, this technique can reduce the cost of obtaining the solution. As with any approximation technique, however, the update method will work best in conditions where the elements being approximated vary linearly and, in actuality, undergo little change.

In general, the elements of the Jacobian will undergo greater change early in the iteration process, where residual error levels are high, than they will later in the calculation as the solution becomes established. Strictly reformulating the Jacobian matrix every three iterations can therefore result not only in unnecessary numerical difficulties early in a calculation (due to inherent approximations affiliated with the update procedure) but also in unnecessary numerical expense late in a calculation (due to Jacobian reformulation when an update would be just as good). Therefore, the Jacobian reformulation frequency was adjusted to be a function of the residual error level. The following approximate schedule was determined from numerical experimentation for the number of iterations employing the update procedure as a function of residual error level:

error range	N_{up}
$E > 0.5$	1
$0.5 \geqslant E > 0.1$	2
$0.1 \geqslant E$	5

Several cases of this study were reanalyzed with the above Jacobian update schedule. Although no cases have been found which required this technique to obtain convergence, calculations with the adjusted Jacobian update schedule evidenced smoother convergence properties than did the baseline calculations. The cost of the modified calculation was comparable to the baseline calculation primarily because the increased Jacobian reformulation frequency at high residual error levels is traded off against the reduced frequency at low levels of error.

A DIRECT APPROACH FOR CAMBERED WINGS

The techniques described in this report can also be used directly to obtain solutions for cases where no prior information is available for use with the partial restart. An example is shown in figure 14 for wings with large camber at freestream conditions where the leading-edge vortex is small and acting on the forward-facing camber surface. The approach, to be subsequently described, will be first applied to the circular-arc conical-camber wings of Barsby (1974) and then to a vortex flap configuration.

Attached flow calculations were first performed with the free-vortex-sheet code to determine the smooth-onflow angle of attack. For these conical wings, this condition occurred along the entire leading edge within an angle of attack of about 1°. The modeling included the short near wake and the calculations incorporated the scheduled Jacobian update procedure. Because the angle of attack differs slightly from the smooth-onflow angle, the leading-edge vortex will be small and governed primarily by properties near the leading edge. To approximate these effects, the initial vortex geometry was based upon the conical flow solution of Smith (1966) for the incremental angle of attack beyond smooth onflow and was rotated by the transverse wing slope at the leading edge.

Calculations were performed for a unit-aspect-ratio wing, first with a nondimensional camber height of 0.4 for freestream conditions 5° above smooth onflow. The calculation readily converged, and some properties of the three-dimensional solution are shown in figure 15a at the wing trailing edge. The simple starting procedure just described provided a reasonable estimate of the converged vortex geometry. For comparison purposes, the flat-plate conical-flow solution is also shown. This solution emphasizes the significant effects camber has on the vortex solution and also indicates probable convergence difficulties if the flat-plate solution were to be used as a starting solution for the cambered wing.

A more extreme case is shown in figure 15b. From the previous calculation ($p = 0.4$) it was apparent that the described starting procedure resulted in an oversized vortex, so the starting vortex geometry for the current calculation ($p = 0.6$) was further scaled down by 50 percent. The calculation readily converged and resulted in an extremely small vortex. As a consequence, this solution exhibited nearly 90-percent suction, based upon the (usual) attached-flow/zero-suction and flat-plate-optimum drag levels.

As a final application, this direct approach was applied to a vortex flap geometry. The resultant convergence histories (figure 16) show the dramatic effects of the new formulation. It should be noted that convergence is displayed at a residual error level of 10^{-6}; as was shown earlier the solution is sufficiently established at a residual level of 10^{-3} for practical purposes.

CONCLUDING REMARKS

A variety of extensions have been implemented to the free-vortex-sheet formulation for the purpose of improving the convergence characteristics of the method. By extending the modeling capability of the code significant improvements in the convergence characteristics were realized without changing the basic numerical scheme. Some results of this study are summarized below.

Only a short near wake is required to capture the significant effects of nonplanar vorticity. The convergence of a calculation with a short near wake is nearly as fast as the convergence of a calculation with no near wake at all. With either wake representation, the solution properties evidenced little variation beyond a residual error level of 10^{-3}.

A "partial restart" was added to the formulation. This allows for the use of an arbitrary vortex from a prior calculation as a starting solution. In addition, simple vortex manipulation features such as rotation and scaling proved to be very effective in enhancing convergence.

With the extensions described in this report, the utility of the FVS formulation has been extended to conditions where the vortex is small. This allows for three-dimensional calculations to be easily performed at low angles of attack and on configurations with highly deflected leading edges.

REFERENCES

Barsby, J. E. (1974): Flow Past Conically-Cambered Slender Delta Wings with Leading-Edge Separation. ARC R&M No. 3748, September.

Blom, G.; Wai, J. C.; and Yoshihara, H. (1985): Viscous Vortical Flow Calculations over Delta Wings. Vortex Flow Aerodynamics - Volume I, NASA CP-2416, paper no. 12, 1986.

Broyden, C. G. (1973): Quasi-Newton or Modification Methods. Numerical Solution of Systems of Nonlinear Algebraic Equations, edited by G. D. Bryne and C. A. Hall, Academic Press, New York.

Brune, G. W.; Weber, J. A.; Johnson, F. T.; Lu, P.; and Rubbert, P. E. (1975): A Three-Dimensional Solution of Flows Over Wings with Leading-Edge Vortex Separation. Part I -- Engineering Document. NASA CR-132709, September.

Brune, G. W.; and Rubbert, P. E. (1977): Boundary Value Problem of Configurations with Compressible Free Vortex Flow. AIAA Journal, pp. 1521-1523, October.

Buter, T. A.; Rao, D. M.; and Schoonover, W. E., Jr. (1985): Experimental and Computational Investigation of an Apex Flap Concept on a 74 Degree Delta Wing. NASA CR-166080, December.

Erickson, G. E. (1983): Application of Free Vortex Sheet Theory to Slender Wings with Leading-Edge Vortex Flaps. AIAA Paper No. 83-1813, July.

Erickson, Gary E. (1985): Vortex/Linear Lift Augmentation. Volume VI--Free Vortex Sheet Computation Study. AFWAL TR-85-3017, June.

Frink, N. T. (1982): Analytical Study of Vortex Flaps on Highly Swept Delta Wings. Proceedings of the 13th Congress of ICAS, Paper No. 82-6.7.2, August.

Frink, N. T. (1986): Critical Evaluation of a Vortex Flap Design Concept Using a 74° Delta Configuration. Vortex Flow Aerodynamics - Volume II, NASA CP-2417, paper no. 2.

Gloss, B. B., and Johnson, F. T. (1976): Development of an Aerodynamic Theory Capable of Predicting Surface Loads on Slender Wings with Vortex Flow. NASA CP-001, pp. 55-67.

Harrison, W. F. (1982): M.A.W. Advanced Leading Edge Devices. Boeing Report No. D180-27024-1, March.

Harrison, W. F. (1982b): Effects of M.A.W. Camber on Vortex Flap Performance. Boeing Report No. D180-27050-1, April.

Hoffler, K. D. (1985): Investigation of the "Vortex Tab." NASA CR-172586, May.

Hummel, D. (1979): On the Vortex Formation Over a Slender Wing at Large Angles of Incidence. AGARD CP-247, Paper No. 15, January.

Johnson, F. T., Lu, P., Brune, G. W., Weber, J. A., and Rubbert, P. E. (1976): An Improved Method for the Prediction of Completely Three-Dimensional Aerodynamic Load Distributions of Configurations with Leading Edge Vortex Separation. AIAA Paper No. 76-417, July.

Johnson, F. T.; Lu, P.; Tinoco, E. N.; and Epton, M. A. (1980): An Improved Panel Method for the Solution of Three-Dimensional Leading-Edge Vortex Flows. Volume I-Theory Document. NASA CR-3278, July.

Kuhlman, J. M. (1978): Analytical Studies of Separated Vortex Flow on Highly Swept Wings. NASA CR-3022, November.

Lamar, J. E. (1978): Subsonic Vortex-Flow Design Study for Slender Wings. AIAA Paper No. 78-154, January.

Lamar, J. E.; and Luckring, J. M. (1979): Recent Theoretical Developments and Experimental Studies Pertinent to Vortex Flow Aerodynamics--With a View Towards Design. AGARD CP-247, Paper No. 24, January.

Luckring, J. M.; Schoonover, W. E., Jr.; and Frink, N. T. (1982): Recent Advances in Applying Free Vortex Sheet Theory for the Estimation of Vortex Flow Aerodynamics. AIAA Paper No. 82-0095.

Luckring, J. M. (1985): A Theory for the Core of a Three-Dimensional Leading Edge Vortex. AIAA Paper No. 85-0108, January.

Luckring, J. M.; Hoffler, K. D.; and Grantz, A. C. (1986): Recent Extensions to the Free-Vortex-Sheet Theory for Expanded Convergence Capability. Vortex Flow Aerodynamics - Volume I, NASA CP-2416, paper no. 4.

Manro, M. E. (1983): Aeroelastic Loads Prediction for an Arrow Wing--Task III -- Evaluation of the Boeing Three-Dimensional Leading-Edge Vortex Code. NASA CR-3642, April.

Polhamus, E. C. (1983): Applications of Slender Wing Benefits to Military Aircraft. AIAA Paper No. 83-2566, October.

Polhamus, E. C. (1985): Vortex Lift Research: Early Contributions and Current Challenges. Vortex Flow Aerodynamics - Volume I, NASA CP-2416, paper no. 1, 1986.

Reddy, C. S. (1979): Theoretical Study of Aerodynamic Characteristics of Wings Having Vortex Flow. NASA CR-159184, November.

Reddy, C. S. (1981): Investigation of Aerodynamic Characteristics of Wings Having Vortex Flow Using Different Numerical Codes. NASA CR-165706, April.

Reddy, C. S. (1981b): Effect of Sweep Angles on Aerodynamic Performance of Double Arrow Wing -- An Analytical Study. Journal of Aircraft, Vol. 18, No. 8, pp. 702-703, August.

Reddy, C. S. (1981c): Effect of Leading-Edge Vortex Flaps on Aerodynamic Performance of Delta Wings. Journal of Aircraft, Vol. 18, No. 9, pp. 796-798, September.

Smith, J. H. B. (1966): Improved Calculations of Leading-Edge Separation from Slender Delta Wings. RAE TR No. 66070, March.

Tinoco, E. N., and Yoshihara, H. (1979): Subcritical Drag Minimization for Highly Swept Wings with Leading Edge Vortices. AGARD CP-247, Paper No. 26, January.

Wai, J. C.; Baille, J.; and Yoshihara, H. (1985): Computation of Turbulent Separated Flows. Third Symposium on Numerical and Physical Aspects of Aerodynamic Flows, January.

Woodson, S. H.; and DeJarnette, F. R. (1985): A Direct and Inverse Boundary Layer Method for Subsonic Flow Over Delta Wings. Vortex Flow Aerodynamics - Volume I, NASA CP-2416, paper no. 5, 1986.

TABLE 1.- CONVERGED FVS PARAMETER SPACE, PUBLISHED RESULTS

(a) delta wings, uncambered

Reference	Planform Class	Λ_1	Λ_2	Λ_{te}	AR	λ	Camber Class	δ_1	Λ_{hl}	δ_2	Thickness Wing	Thickness Fusl	Vortex Span	Flow α	β	M
Brune, et al. (1975)	Delta	70	-	0	1.46	0	Flat	-	-	-	Thin	-	Full	9-19	0	0
		76	"	"	1.00	"	"	"	"	"	"	"	"	10-20	"	"
Brune, et al. (1977)	Delta	74	-	0	1.15	0	Flat	-	-	-	Thin	-	Full	5-20	0	0.8
Buter, et al. (1985)	Delta	74	-	0	1.15	0	Flat	-	-	-	Thin	-	Full	10	0	0
Erickson (1983)	Delta	55	-	0	2.80	0	Flat	-	-	-	Thin	-	Full	15	0	0.6
		65	"	"	1.87	"	"	"	"	"	"	"	"	"	"	"
		"	"	"	"	"	"	"	"	"	"	"	Part	"	"	"
		75	"	"	1.07	"	"	"	"	"	"	"	Full	"	"	"
Gloss, et al. (1976)	Delta	63.4	-	0	2.00	0	Flat	-	-	-	Thin	-	Full	20	0	0
		70	"	"	1.46	"	"	"	"	"	"	"	"	14	"	"
Hoffler (1985)	Delta	65	-	0	1.87	0	Flat	-	-	-	Thin	-	Full	16	0	0
Johnson, et al. (1976)	Delta	70	-	0	1.46	0	Flat	-	-	-	Thin	-	Full	14	0	0
		74	"	"	1.15	"	"	"	"	"	"	"	"	5-25	"	0.6
Johnson, et al. (1980)	Delta	63.4	-	0	2.00	0	Flat	-	-	-	Thin	-	Full	20	0	0
		70	"	"	1.46	"	"	"	"	"	"	"	"	14	"	"
		74	"	"	1.15	"	"	"	"	"	"	"	"	15-30	"	"
		76	"	"	1.00	"	"	"	"	"	"	"	"	20	"	"
		80	"	"	0.71	"	"	"	"	"	"	"	"	15	5	"
		86.4	"	"	0.25	"	"	"	"	"	"	"	"	2-25	0	"
		63-86	"	"	2-0.25	"	"	"	"	"	"	"	"	20	"	"
Kuhlman (1978)	Delta	63-86	-	0	2-0.25	0	Flat	-	-	-	Thin	-	Full	15	0	0
		63-80	"	"	2-0.71	"	"	"	"	"	"	"	"	20	"	"
		82.7	"	"	0.52	"	"	"	"	"	"	"	"	10-40	"	0.8
		"	"	"	"	"	"	"	"	"	"	"	"	10.3	"	0.7
		"	"	"	"	"	"	"	"	"	"	"	"	30	"	"
		"	"	"	"	"	"	"	"	"	"	"	"	20.8	"	0.5-0.8
Lamar (1978)	Delta	74	-	0	1.15	0	Flat	-	-	-	Thin	-	Full	15-25	0	0
		80	"	"	0.71	"	"	"	"	"	"	"	"	10-25	"	"
Lamar, et al. (1979)	Delta	74	-	0	1.15	0	Flat	-	-	-	Thin	-	Full	20	10	0.2
Luckring, et al. (1982)	Delta	63	-	0	2.04	0	Flat	-	-	-	Thin	-	Full	20	0	0.3
		74	"	"	1.15	"	"	"	"	"	"	"	"	10-25	0,5	0.2
		"	"	"	"	"	"	"	"	"	"	"	"	20	0,15	"
		82.7	"	"	0.52	"	"	"	"	"	"	"	"	10	0	0.99
		"	"	"	"	"	"	"	"	"	"	"	"	20.8	0	0-0.99
Luckring, et al. (1985b)	Delta	65	-	0	1.87	0	Flat	-	-	-	Thin	-	Full	15	0	0
Polhamus (1983)	Delta	70	-	0	1.46	0	Flat	-	-	-	Thin	-	Full	10-50	0	0
		80	"	"	0.71	"	"	"	"	"	"	"	"	5-50	"	"
Polhamus (1985)	Delta	70	-	0	1.46	0	Flat	-	-	-	Thin	-	Full	10-50	0	0
		76	"	"	1.00	"	"	"	"	"	Thick	"	"	25	"	"
		80	"	"	0.71	"	"	"	"	"	Thin	"	"	5-50	"	"
Reddy (1979)	Delta	70	-	0	1.46	0	Flat	-	-	-	Thin	-	Full	10-30	0	0
		76	"	"	1.00	"	"	"	"	"	"	"	"	5-30	"	"
Reddy (1981)	Delta	70	-	0	1.46	0	Flat	-	-	-	Thin	-	Full	15-40	0	0

TABLE 1.- CONTINUED

(b) arrow and diamond wings, uncambered

Reference	Planform Class	Λ_1	Λ_2	Λ_{te}	AR	λ	Camber Class	δ_1	Λ_{hl}	δ_2	Thickness Wing	Thickness Fusl	Vortex Span	Flow α	β	M
Brune, et al. (1975)	Arrow	71.2	-	43.6	2.02	0	Flat	-	-	-	Thin	-	Full	15.8	0	0
Brune, et al. (1977)	Arrow	74	-	37	1.47	0	Flat	-	-	-	Thin	-	Full	5-25	0	0.6
Johnson, et al. (1976)	Arrow	71.2 74	- "	43 37	2.00 1.47	0 "	Flat "	- "	- "	- "	Thin "	- "	Full "	11.9 5-25	0 "	0.4 0.6
Johnson, et al. (1980)	Arrow	71.2	-	43	2.00	0	Flat	-	-	-	Thin	-	Full	11.9	0	0.4
Kuhlman (1978)	Arrow	70	-	36.9	2.00	0	Flat	-	-	-	Thin	-	Full	10-30	0	0
Luckring, et al. (1982)	Arrow +	67	-	55	2.50	0	Flat	-	-	-	Thin	-	Full	7-14	0	0.76
Polhamus (1983)	Arrow	70	-	36.9	2.00	0	Flat	-	-	-	Thin	-	Full	5-50	0	0
Reddy (1979)	Arrow	70 " "	- " "	36.9 28.8 15.4	2.00 1.82 1.62	0 " "	Flat " "	- " "	- " "	- " "	Thin " "	- " "	Full " "	15-40 " "	0 " "	0 " "
Kuhlman (1978)	Diamond	70	-	-51.3	1.00	0	Flat	-	-	-	Thin	-	Full	10-30	0	0
Reddy (1979)	Diamond	70 " " " "	- " " " "	-15.4 -28.8 -39.5 -47.7 -51.3	1.32 1.21 1.12 1.04 1.00	0 " " " "	Flat " " " "	- " " " "	- " " " "	- " " " "	Thin " " " "	- " " " "	Full " " " "	15-40 " " " "	0 " " " "	0 " " " "
Reddy (1981)	Diamond	70	-	-51.3	1.00	-	Flat	-	-	-	Thin	-	Full	25-40	0	0

+ B-1 Planform

TABLE 1.- CONTINUED

(c) cropped wings, uncambered

Reference	Planform Class	Λ_1	Λ_2	Λ_{te}	AR	λ	Camber Class	δ_1	Λ_{hl}	δ_2	Thickness Wing	Thickness Fusl	Vortex Span	Flow α	β	M
Erickson (1983)	Cropped Delta	65	-	0	2.80	0.25	Flat	-	-	-	Thin	-	Full	15	0	0.6
Erickson (1985)	Cropped Delta	55	-	0	1.80	0.2	Flat	-	-	-	Thin	-	Full	15	0	0.4
Luckring, et al. (1982)	Cropped Delta	63	-	0	0.87	0.4	Flat	-	-	-	Thin	-	Full	20	0	0.3
Reddy (1981)	Cropped Delta	63 80	- "	0 "	0.87 0.27	0.4 0.45	Flat "	- "	- "	- "	Thin "	- "	Full "	15-25 15-35	0 "	0.2 0
Manro (1983)	Cropped Arrow	71.2 " " " "	- " " " "	43 " " " "	1.65 " " " "	0.1 " " " "	Flat " " " "	- " " " "	- " " " "	- " " " "	Thin Thick " " Thin	- " Thick - "	Full " " Part "	16 " " 8 6	0 " " " "	0.4 " " " "
Reddy (1981)	Cropped Arrow	63	-	40	1.07	0.4	Flat	-	-	-	Thin	-	Full	15-25	0	0.2
Reddy (1981)	Cropped Diamond	63	-	-40	0.74	0.4	Flat	-	-	-	Thin	-	Full	15-25	0	0.2

(d) cranked wings, uncambered

Reference	Planform Class	Λ_1	Λ_2	Λ_{te}	AR	λ	Camber Class	δ_1	Λ_{hl}	δ_2	Thickness Wing	Thickness Fusl	Vortex Span	Flow α	β	M
Erickson (1983)	Cranked Delta	72	62	0	1.68	0	Flat	-	-	-	Thin	-	Full	15	0	0
Kuhlman (1978)	Cranked Delta	80	65	0	1.60	0	Flat	-	-	-	Thin	-	Full	5-30	0	0
Reddy (1981)	Cranked Delta	80 "	65 "	0 "	1.60 0.95	0 0.2	Flat "	- "	- "	- "	Thin "	- "	Full "	15-30 "	0 "	0 "
Reddy (1981)	Cranked Arrow	80 "	65 "	30 "	2.08 1.10	0 0.23	Flat "	- "	- "	- "	Thin "	- "	Full "	15-25 15-30	0 "	0 "
Reddy (1981b)	Cranked Arrow	70-80 80	65 60-70	30 "	2.6-2.1 2.6-1.6	0 "	Flat "	- "	- "	- "	Thin "	- "	Full "	20 "	0 "	0 "

TABLE 1.- CONTINUED

(e) miscellaneous wings, uncambered

Reference	Planform Class	Λ_1	Λ_2	Λ_{te}	AR	λ	Camber Class	δ_1	Λ_{hl}	δ_2	Thickness Wing	Thickness Fusl	Vortex Span	Flow α	β	M
Brune, et al. (1975)	Gothic Arrow	50	87	56.3	1.60	0	Flat	-	-	-	Thin	-	Full	14.3	0	0
Erickson (1983)	Gothic	62.5	76.6	0	1.35	0	Flat	-	-	-	Thin	-	Full	15	0	0
Frink (1985)	Gothic	60	74	0	1.36	0	Flat	-	-	-	Thin	Thin	Part	10-16	0	0
		"	"	"	"	"	"	"	"	"	"	Thick	Full	14	"	"
Johnson, et al. (1980)	Rectangle	0	-	0	0.2-1.2	1	Flat	-	-	-	Thin	-	Full	20	0	0.2
Reddy (1981)	Raked Side Edge	63	-3-13	0	1.07	0.4	Flat	-	-	-	Thin	-	Full	23	0	0

(f) all planforms, conventional camber

Reference	Planform Class	Λ_1	Λ_2	Λ_{te}	AR	λ	Conventional Camber Class	$\delta 1$	Λhl	$\delta 2$	Thickness Wing	Thickness Fusl	Vortex Span	Flow α	β	M
Buter, et al. (1985)	Delta	74	-	0	1.15	0	Apex Flap	0-40	-	-	Thin	-	Full	10	0	0
		"	"	"	"	"	"	20	"	"	"	"	Inbd	"	"	"
Luckring, et al. (1985b)	Delta	76	-	0	1.00	0	T.E. Flap	-6	-	-	Thin	-	Full	-20-50	0	0
Reddy (1981)	Delta	75	-	0	1.07	0	Smooth Onflow, Cld = 0.3	-	-	-	Thin	-	Full	2-30	0	0
Johnson, et al. (1980)	Arrow	71.2	-	43	1.65	0	T.E. Flap	8.3	-	-	Thin	-	Full	11.9	0	0.4
Manro (1983)	Cropped Arrow	71.2	-	43	1.65	0.1	Twist	-	-	-	Thin	-	Full	16	0	0.4
		"	"	"	"	"	Twist/Camber	"	"	"	"	"	"	"	"	"
Harrison (1982b)	Cranked Arrow +	70	58	48	2.24	0	L. E. Droop	0-15	58	-	Thin	-	Part	20-25	0	0.65

+ AFTI/F-111 Planform and Camber

TABLE 1.- CONTINUED

(g) all planforms, conical camber

Reference	Planform Class	Λ_1	Λ_2	Λ_{te}	AR	λ	Conical Camber Class	δ_1	Λ_{h1}	δ_2	Thickness Wing	Thickness Fusl	Vortex Span	Flow α	β	M
Johnson, et al. (1980)	Delta	74	-	0	1.15	0	Wentz	-	-	-	Thin	-	Full	10-31	0	0
Kuhlman (1978)	Delta	74	-	0	1.15	0	Wentz	-	-	-	Thin	-	Full	10-31	0	0
Lamar (1978)	Delta	74	-	0	1.15	0	Wentz	-	-	-	Thin	-	Full	15-25	0	0
		80	"	"	0.71	"	Barsby, p=0.2	"	"	"	"	"	"	10-25	"	"
		"	"	"	"	"	Barsby, p=0.4	"	"	"	"	"	"	15-25	"	"
Luckring, et al. (1985b)	Delta	76	-	0	1.00	0	Barsby, p=0.4	-	-	-	Thin	-	Full	14	0	0
		"	"	"	"	"	Barsby, p=0.6	"	"	"	"	"	"	20	"	"
Reddy (1979)	Delta	76	-	0	1.00	0	Nangia Wing E	-	-	-	Thin	-	Full	10-30	0	0
		"	"	"	"	"	Squire Wing 1	"	"	"	"	"	"	10-40	"	"
		"	"	"	"	"	Squire Wing 2	"	"	"	"	"	"	15-40	"	"
		"	"	"	"	"	Squire Wing 3	"	"	"	"	"	"	"	"	"
		"	"	"	"	"	Squire Wing 4	"	"	"	"	"	"	"	"	"
		"	"	"	"	"	Squire Wing 5	"	"	"	"	"	"	30-40	"	"
Reddy (1981)	Delta	76	-	0	1.00	0	Nangia Wing B	-	-	-	Thin	-	Full	24,30	0	0
		"	"	"	"	"	Squire Wing 4	"	"	"	"	"	"	15-40	"	"
		"	"	"	"	"	Squire Wing 5	"	"	"	"	"	"	20,30	"	"
		"	"	"	"	"	Squire Wing 6	"	"	"	"	"	"	20,30	"	"
Tinoco, et al. (1979)	Delta	74	-	0	1.15	0	Linear Twist	10	-	-	Thin	-	Full	16-30	0	0
		"	"	"	"	"	"	20	"	"	"	"	"	17-30	"	"
		"	"	"	"	"	Wentz/Tabbed	-	"	"	"	"	"	15-30	"	"

TABLE 1.- CONCLUDED

(h) all planforms, vortex-flap camber

Reference	Planform Class	Λ_1	Λ_2	Λ_{te}	AR	λ	Vortex Flap Camber Class	δ_1	Λ_{hl}	δ_2	Thickness Wing	Thickness Fusl	Vortex Span	Flow α	β	M
Erickson (1983)	Delta	65	-	0	1.87	0	Conical	-15-40	74	-	Thin	-	Full	15	0	0.6
		"	"	"	"	"	"	15	"	"	"	"	"	11	"	"
		"	"	"	"	"	"	20	"	"	"	"	"	15-20	"	"
		"	"	"	"	"	"	30	"	"	"	"	"	15	"	0
		"	"	"	"	"	Inverse Taper	15	"	"	"	"	Part	"	"	0.6
	Cranked Delta	72	62	"	1.68	"	"	15	77/70	"	"	"	Full	10,15	"	0.6
Erickson (1985)	Delta	55	-	0	2.80	0	Tapered Chord	0-30	53	0-10	Thin	-	Full	10-30	0-20	0.4
Frink (1982)	Delta	74	-	0	1.15	0	Constant Chord	10	74	-	Thin	-	Full	14	0	0
		"	"	"	"	"	"	"	"	"	"	"	Part	"	"	"
		"	"	"	"	"	"	0-20	"	"	"	"	"	"	"	0.3
		"	"	"	"	"	Conical	20	79	"	"	"	Full	11-20	"	"
Frink (1985)	Gothic	60	74	0	1.36	0	Gothic	30	74	-	Thin	Thin	Part	11-19	0	0
		"	"	"	"	"	"	40	"	"	"	"	"	15-21	"	"
		"	"	"	"	"	"	30	"	"	"	Thick	Full	14,15	"	"
Harrison (1982)	Cranked Arrow +	70	58	48	2.24	0	Tapered Flap A	15-45	58	-	Thin	-	Part	15-25	0	0.65
		"	"	"	"	"	Tapered Flap B	25-35	"	"	"	"	"	"	"	"
		"	"	"	"	"	Tapered Flap C	30	"	"	"	"	"	"	"	"
		"	"	"	"	"	Tapered Flap D	30	"	"	"	"	"	"	"	"
		"	"	"	"	"	Tapered Flap E	30	"	"	"	"	"	"	"	"
		"	"	"	"	"	Twisted Flap B	35/25	"	"	"	"	"	20,25	"	"
		"	"	"	"	"	"	25/35	"	"	"	"	"	"	"	"
		"	"	"	"	"	"	40/30	"	"	"	"	"	"	"	"
		"	"	"	"	"	"	45/30	"	"	"	"	"	"	"	"
		"	"	"	"	"	"	35/45	"	"	"	"	"	"	"	"
		"	"	"	"	"	"	45/35	"	"	"	"	"	20	"	"
		"	"	"	"	"	Apex 2, Flap A	30	"	"	"	"	"	20-25	"	"
		"	"	"	"	"	Apex 3, Flap A	"	"	"	"	"	"	"	"	"
		"	65	55	1.64	"	Tapered Flap A	"	"	"	"	"	"	20,25	"	"
		"	"	"	"	"	Tapered Flap B	"	"	"	"	"	"	"	"	"
		"	58	48	2.24	"	"	0-30	"	"	"	"	"	25	"	"
Harrison (1982b)	Cranked Arrow +	70	58	48	2.24	0	Flap D, L. E. Droop	35	58	0-23	Thin	-	Part	20-25	0	0.65
		"	"	"	"	"										
Hoffler (1985)	Delta	65	-	0	1.87	0	Conical/Tabbed	0-30	74	0-30	Thin	-	Full	16	0	0.1
Luckring, et al. (1982)	Delta	72	-	0	1.30	0	Conical	13	78	-	Thin	-	Full	14	0	0.2
		74	"	"	1.15	"	"	0-25	79	"	"	"	"	"	"	0
		"	"	"	"	"	"	20	76-80	"	"	"	"	"	"	"
		"	"	"	"	"	"	"	79	"	"	"	"	11-20	"	"
		"	"	"	"	"	Constant Chord	"	74	"	"	"	"	14	"	0.3
Reddy (1981c)	Delta	74	-	0	1.15	0	Constant Chord	-30	74	-	Thin	-	Full	15-20	0	0
		"	"	"	"	"	Tapered Chord	24	71.4	"	"	"	"	15-35	"	"
		"	"	"	"	"	"	-60-35	"	"	"	"	"	20.6	"	"

+ AFTI/F-111 Planform and Camber

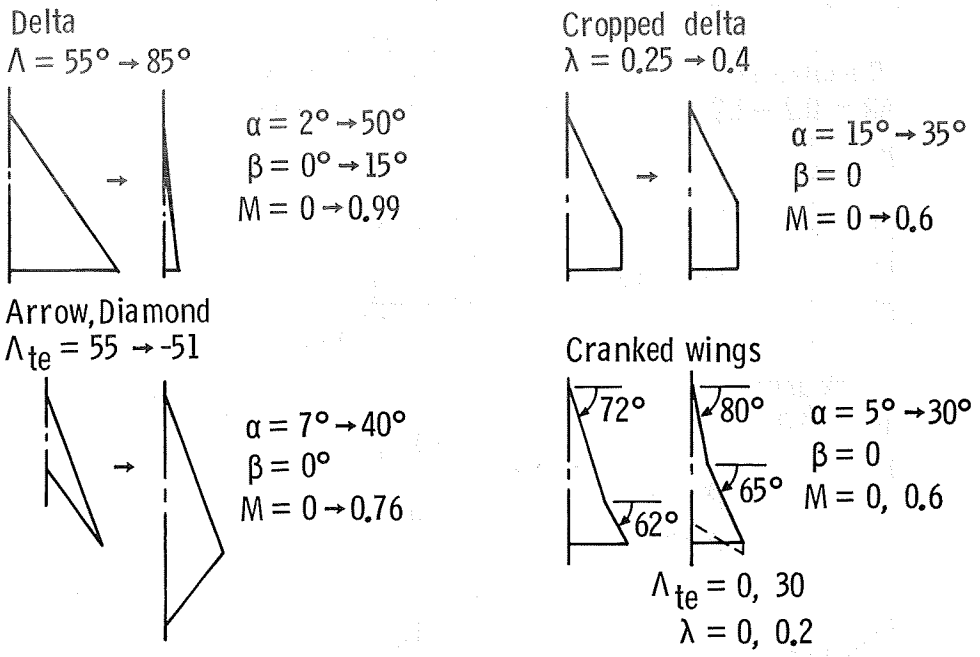

(a) flat wings

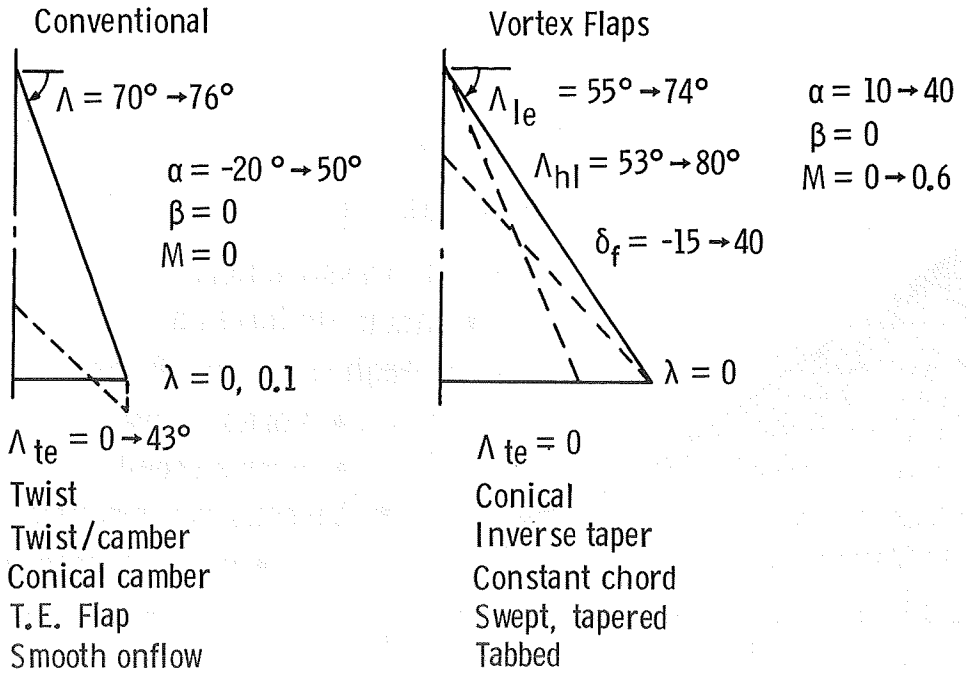

(b) cambered wings

Figure 1.- Converged FVS parameter space. Published results.

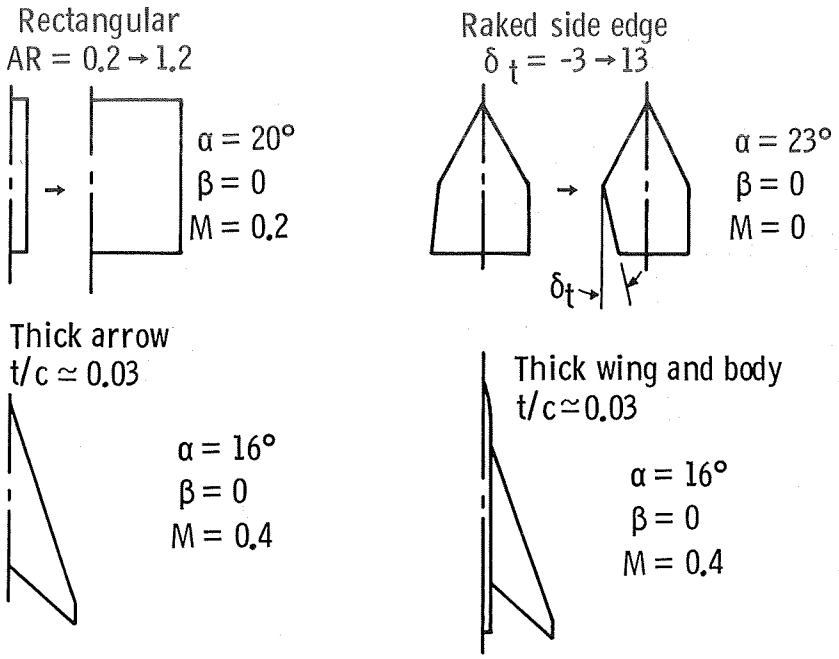

(c) other wings

Figure 1.- Concluded.

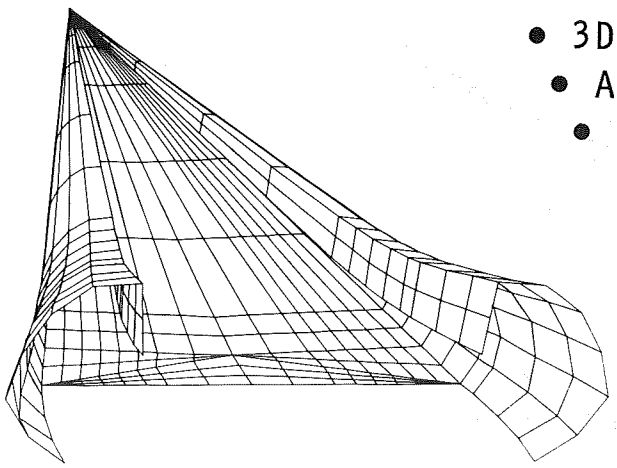

Vortex modeling → Real flow effects

- 3D pressure field
- Accurate forces and moments
- High -α vortex lift loss
  - Vortex curvature
  - Vortex crowding
- Viscous flow extensions
  - Vortex breakdown
  - Secondary separation

Figure 2.- General solution features.

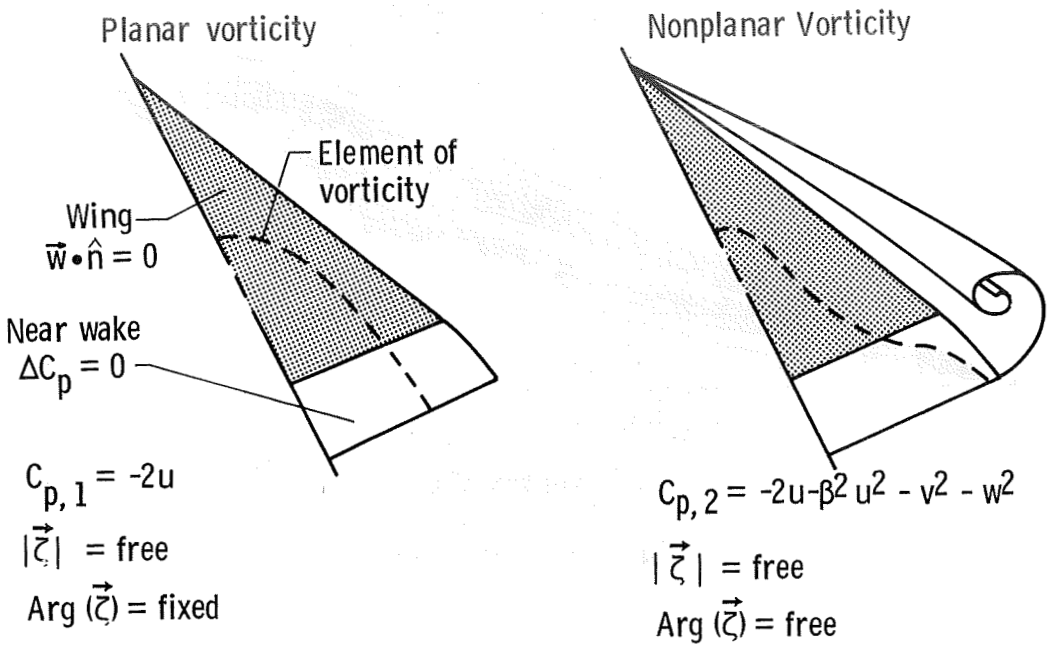

Figure 3.- Near-field wake attributes.

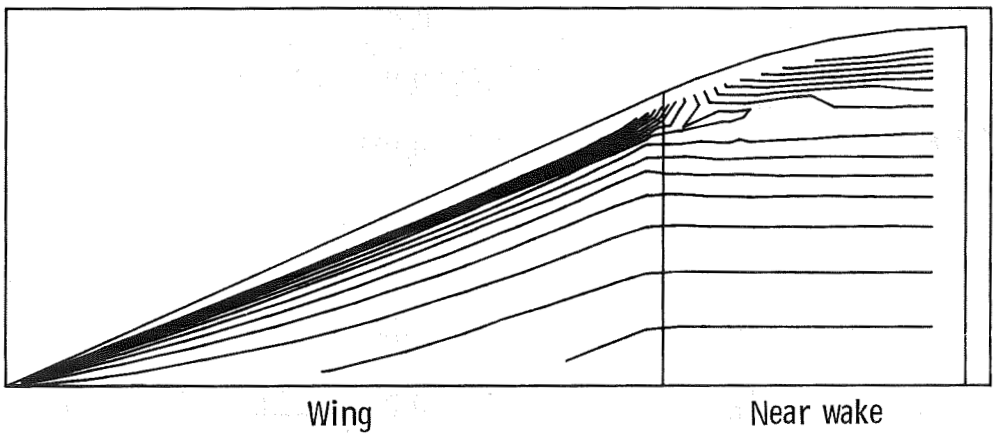

(a) attached flow

Figure 4.- Vorticity contours. $\Lambda = 65°$, $\alpha = 15°$, M = 0, increment = 0.1.

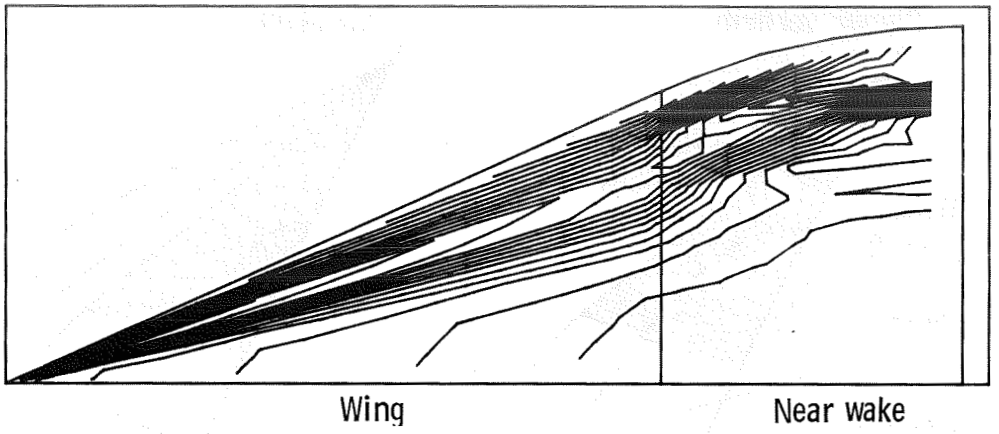

(b) vortex flow

Figure 4.- Concluded.

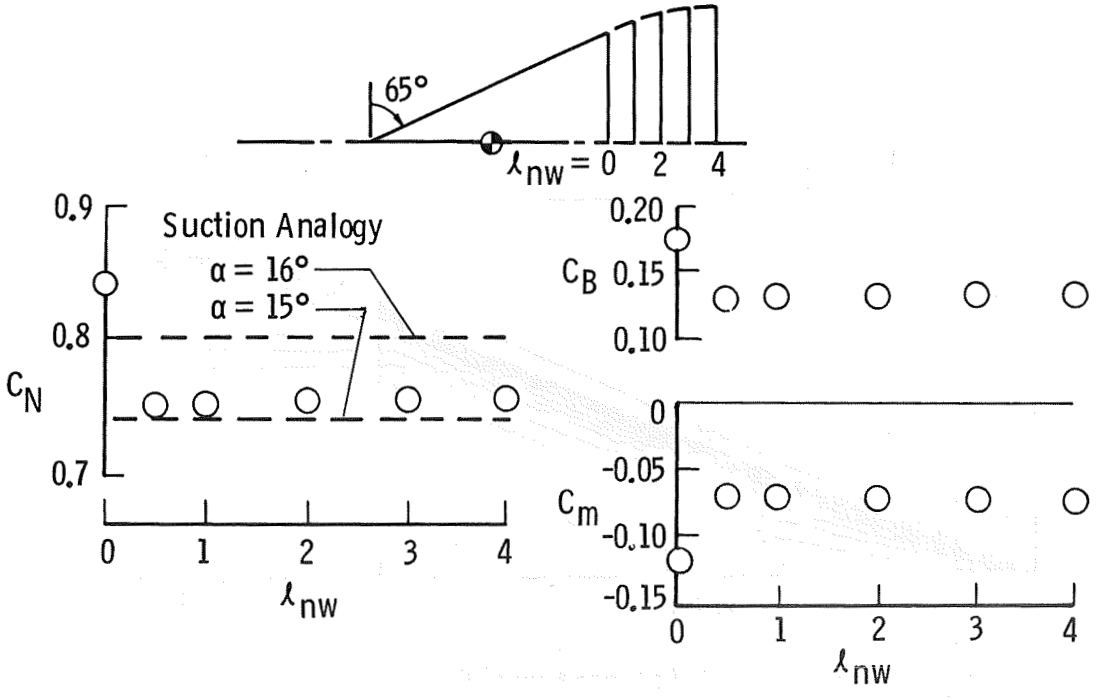

Figure 5.- Near-field wake length effects. α = 15°, M = 0.

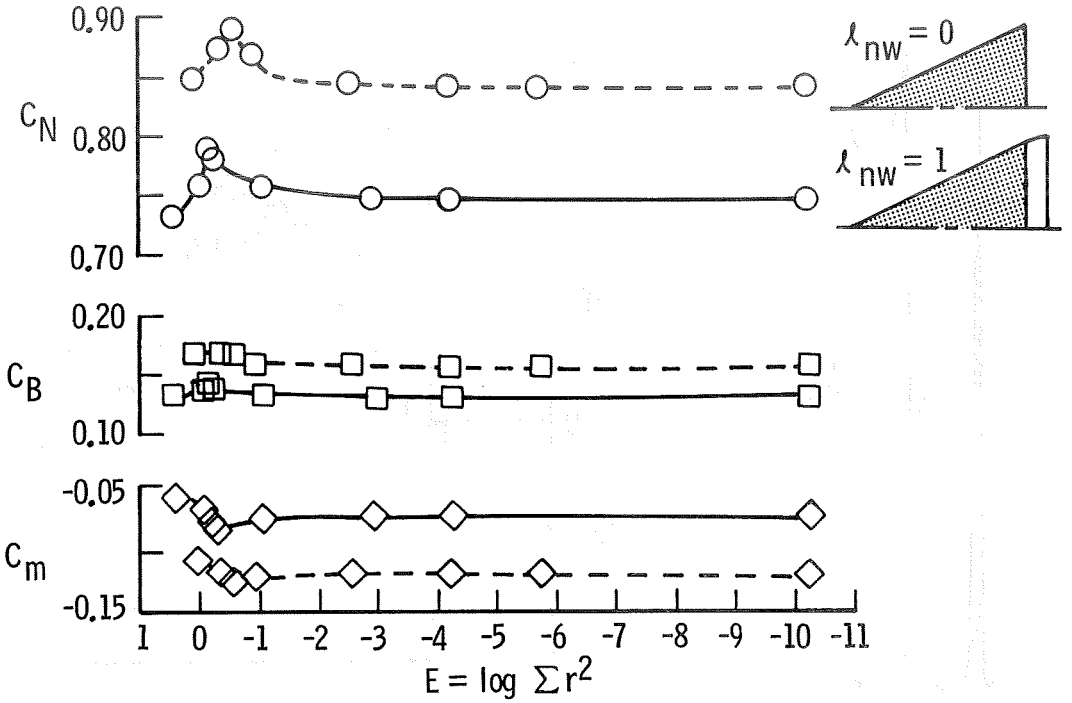

Figure 6.- Convergence histories.

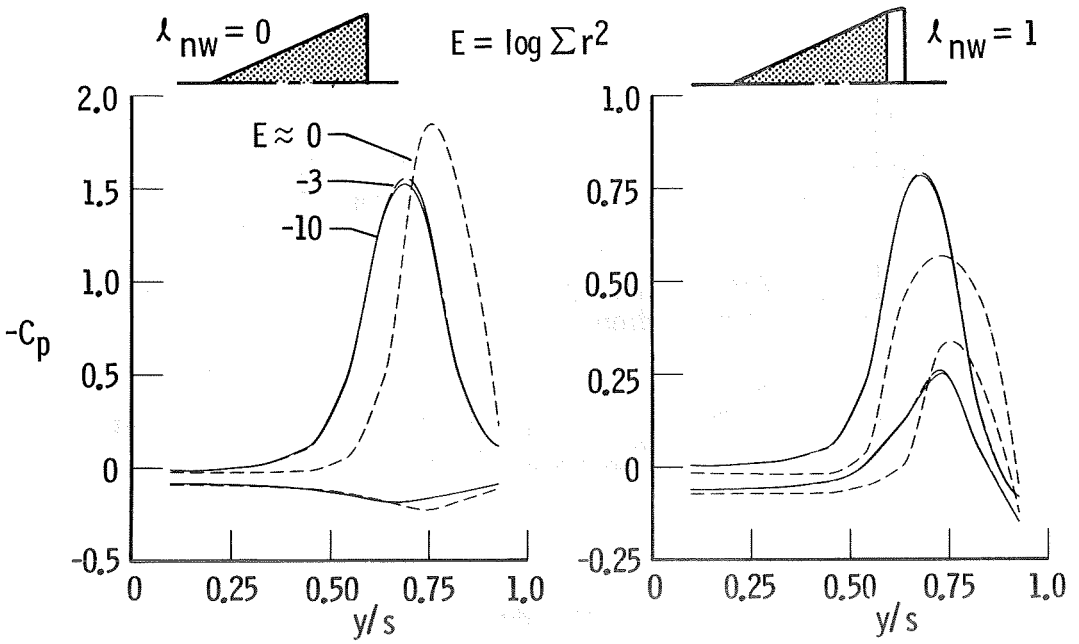

Figure 7.- Convergence effects on spanwise pressures. $x/c_r = 0.975$, $\Lambda = 65°$, $\alpha = 15°$, $M = 0$.

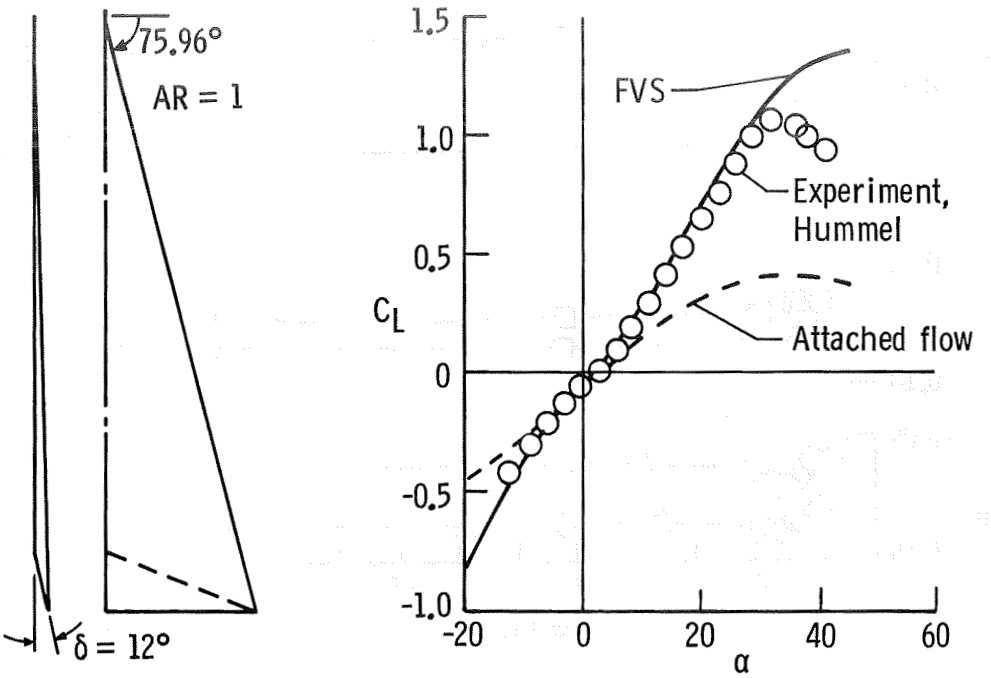

(a) lift

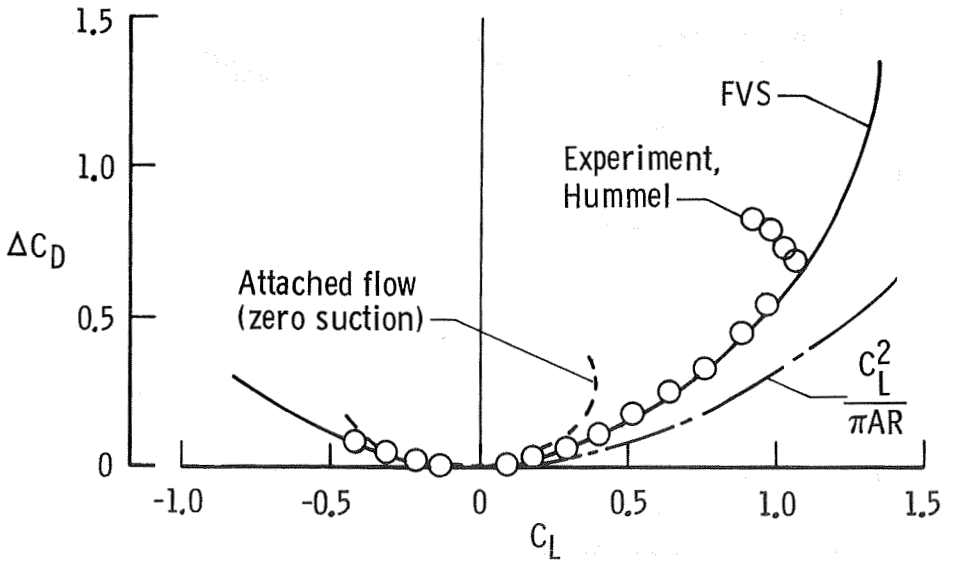

(b) drag

Figure 8.- Force and moment correlation for Hummel delta wing.

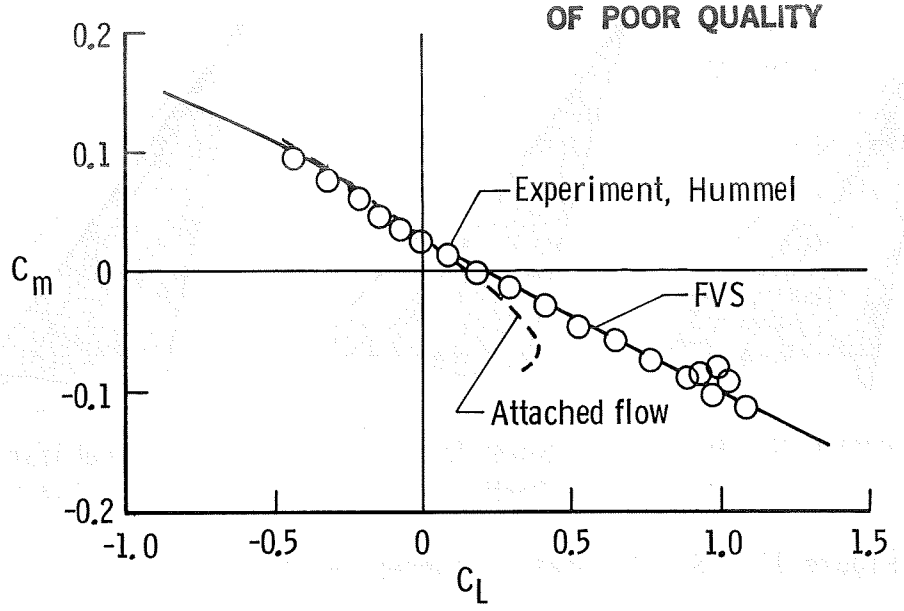

(c) pitching moment

Figure 8.- Concluded.

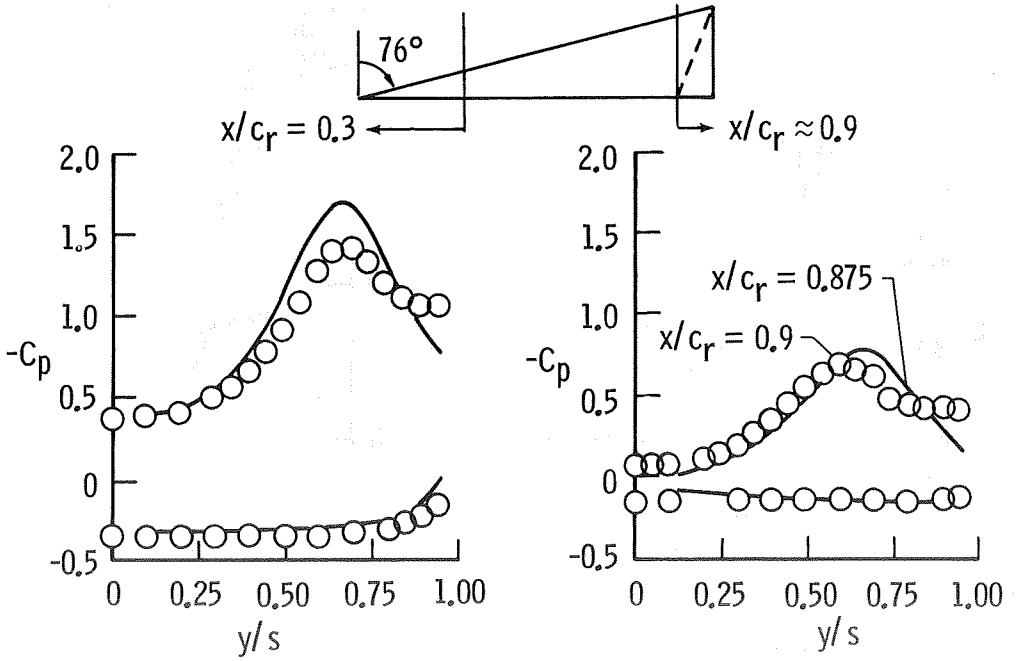

Figure 9.- Spanwise pressure correlation for Hummel delta wing.

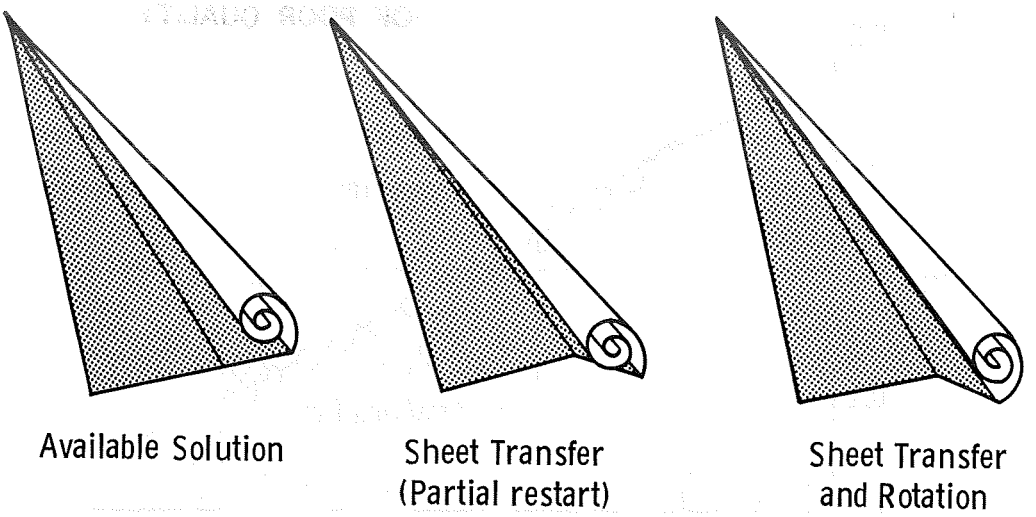

Figure 10.- Sheet rotation concept with partial restart.

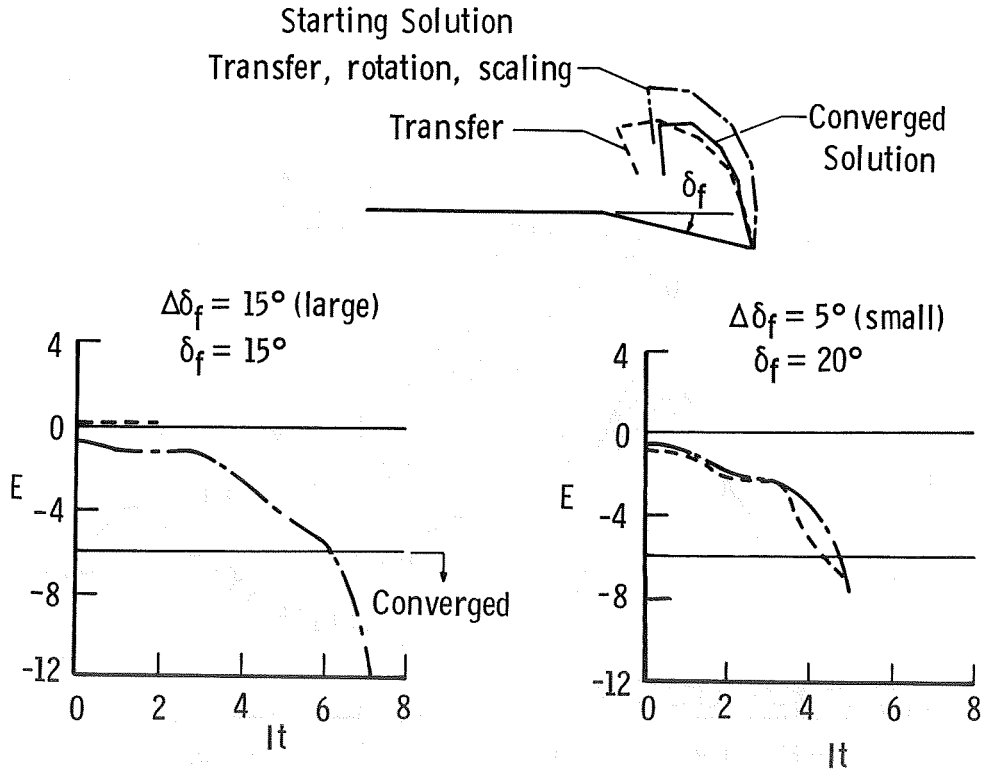

(a) rotation; $\Lambda = 65°$, $\Lambda_{hl} = 74°$, $\alpha = 16°$, $M = 0$

Figure 11.- Effect of vortex sheet manipulation.

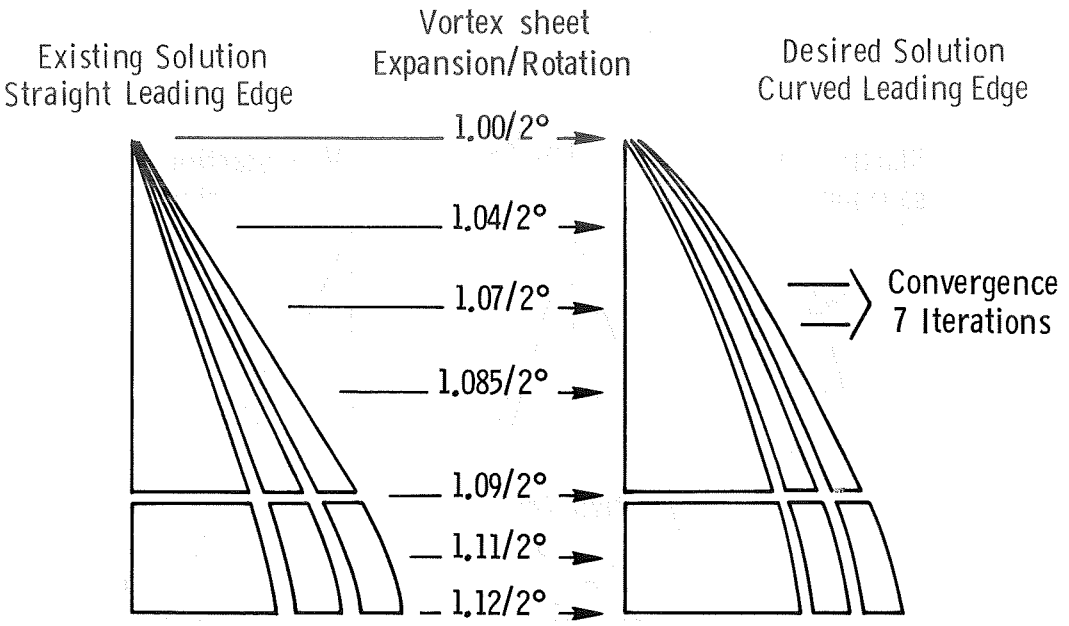

(b) scaling; Λ = 74°, α = 21°, M = 0

Figure 11. Concluded.

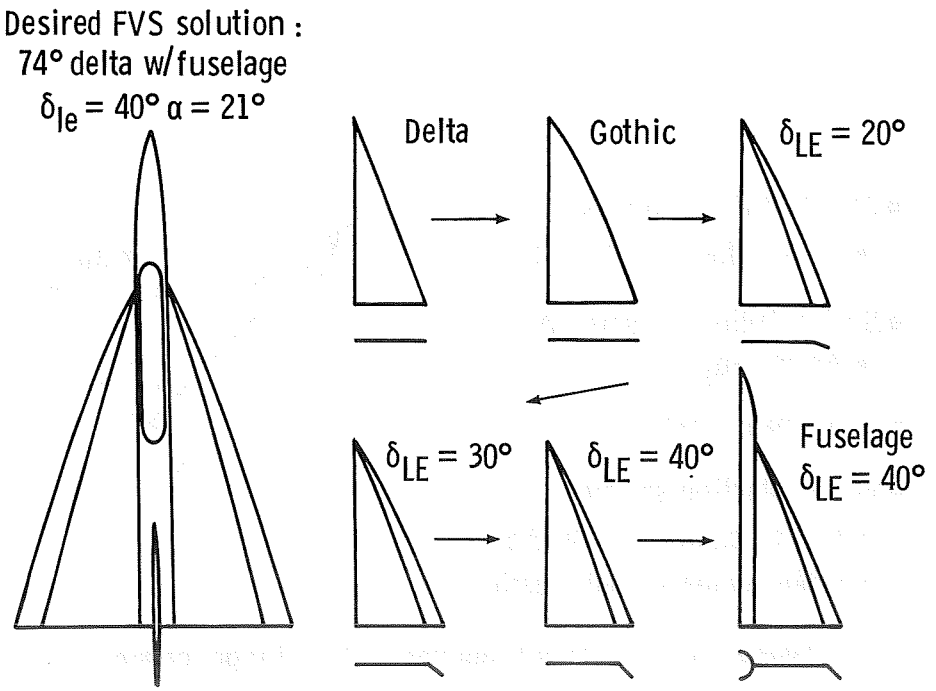

Figure 12.- Application of expanded restart to complex geometries.

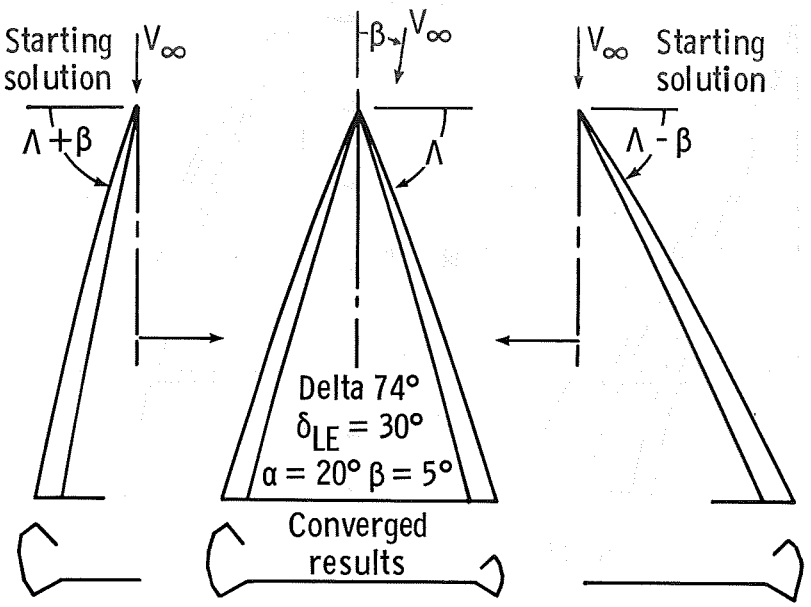

Figure 13.- Multiple vortex sheet partial restart.

- Attached flow analysis
  - $\alpha_{so} = \alpha$ for smooth onflow
- Seek solution for small $\Delta\alpha$
  - $\Delta\alpha = \alpha - \alpha_{so}$
- Short near wake
- Vortex starting solution
  - size by conical flow at $\Delta\alpha$
  - rotate by leading edge deflection

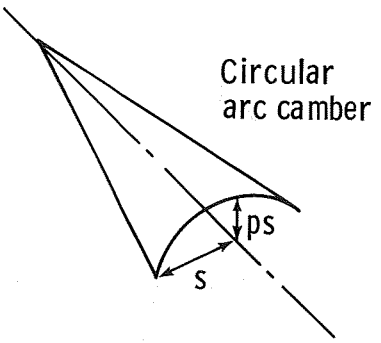

Barsby (1974)

Figure 14.- A direct approach for large camber.

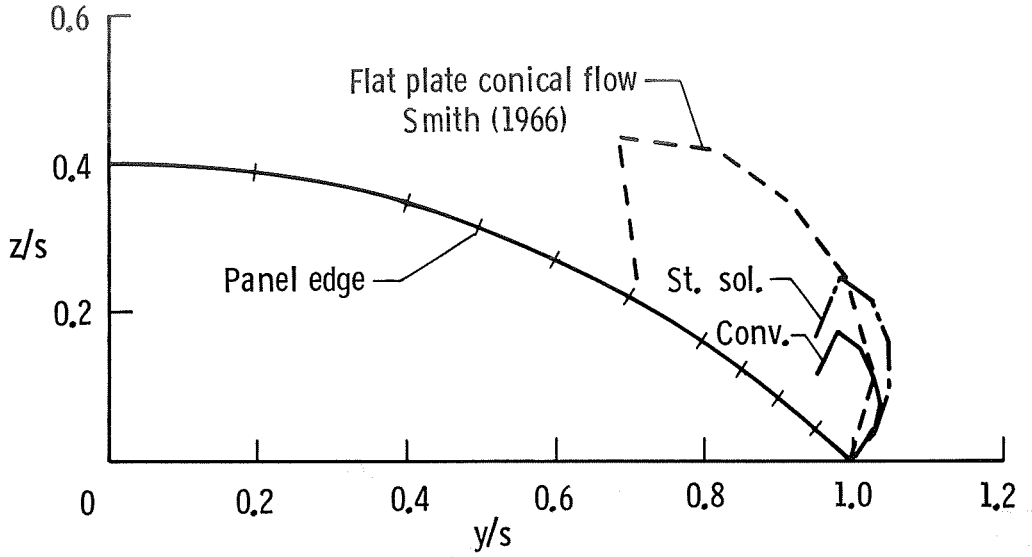

(a) p = 0.4, $\alpha \approx 14°$, $\alpha_{so} \approx 9°$

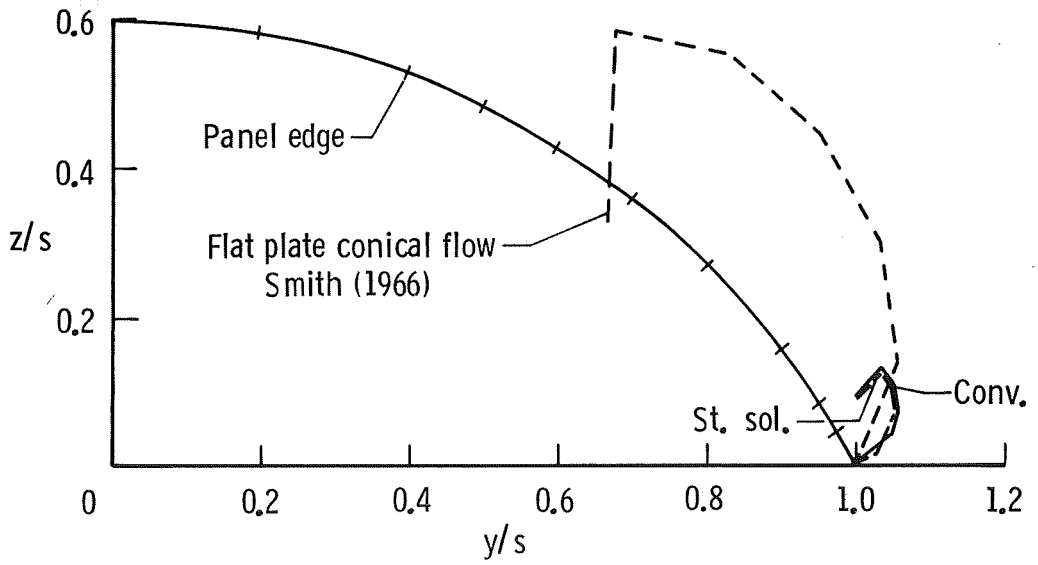

(b) p = 0.6, $\alpha = 20°$, $\alpha_{so} \approx 14°$

Figure 15.- Converged results at trailing edge. AR = 1.

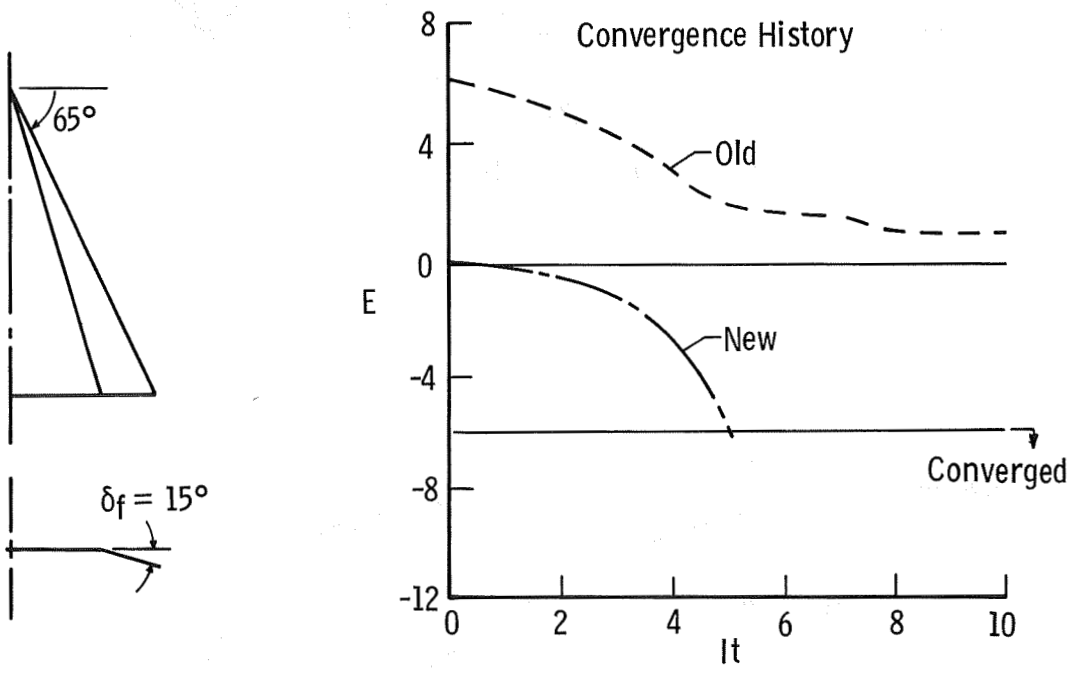

Figure 16.- Application for vortex flap. α = 16°.